Measured and Calculated Airloads on a Transport Wing Model

William E. McCain*
NASA Langley Research Center, Hampton, Virginia

Wind tunnel measurements of steady and unsteady pressures for a high-aspect-ratio supercritical wing model are compared with calculations by the linear unsteady aerodynamic lifting-surface theory, known as the doublet lattice method, at Mach numbers of 0.60 (subsonic) and 0.78 (transonic). The steady-pressure data comparisons are made for incremental changes in angle of attack and control-surface deflection. The unsteady-pressure data comparisons are made for oscillating control-surface deflections. Some differences between the measured and calculated aerodynamics are attributed to viscous and transonic effects not accounted for in the doublet lattice analysis. Comparisons of the transonic unsteady-pressure data for the oscillating control surfaces are improved by applying empirical corrections, based on the steady-pressure measurements, to the unsteady doublet lattice calculations.

Nomenclature

AR = aspect ratio, b^2/S
$b/2$ = wing semispan, m
c = streamwise local chord, m
c_{av} = wing average chord, m
c_ℓ = section lift coefficient
$c_r/2$ = wing root semichord, m
C_p = pressure coefficient
C'_p = lifting-surface steady-pressure coefficient, $C_{p_{l.s.}} - C_{p_{u.s.}}$
$\Delta c_\ell/\Delta\alpha$ = increment in section lift coefficient per change in angle of attack, deg^{-1}
$\Delta c_\ell/\Delta\delta$ = increment in section lift coefficient per change in control-surface deflection, deg^{-1}
$\Delta C'_p/\Delta\alpha$ = increment in lifting-surface pressure coefficient per change in angle of attack, deg^{-1}
$\Delta C'_p/\Delta\delta$ = increment in lifting-surface pressure coefficient per change in control-surface deflection, deg^{-1}
$|C'_p|$ = magnitude of lifting-surface unsteady-pressure coefficient
f = frequency of oscillating control surface, Hz
k = reduced frequency, $c_r\omega/2V$
M = freestream Mach number
q = freestream dynamic pressure, kPa
R = Reynolds number based on wing average chord
S = total wing planform area, m^2
V = freestream velocity, m/s
x = streamwise coordinate, m
x/c = fraction of local streamwise chord
y = spanwise coordinate, m
z = vertical coordinate, positive up, m
α = wing angle of attack, deg
δ = control-surface deflection angle, positive trailing edge down, deg
$\Delta\alpha$ = change in wing angle of attack, deg
$\Delta\delta$ = change in control-surface deflection angle, deg
η = fraction of semispan, $2y/b$
Λ = leading-edge sweepback angle, deg
ϕ = phase angle of unsteady pressure, referenced to control-surface motion (negative for pressure changes lagging the control-surface motion)
ω = circular frequency of oscillating control surface, rad/s

Subscripts

l.s. = lower surface
ref = reference
u.s. = upper surface

Introduction

THE combination of active controls with advanced aerodynamic features such as winglets and supercritical airfoils can provide substantial improvements in aircraft performance, resulting in energy-efficient configurations. The design and analysis of aircraft equipped with relaxed static stability, load alleviation, and flutter suppression systems require the use of multipurpose computer programs. Some of the programs currently used at the NASA Langley Research Center for the synthesis and analysis of active control systems include ISAC,[1] SYNPAC,[2] DYLOFLEX,[3] and the aerodynamic energy method,[4] all of which use the linear lifting-surface aerodynamics of the doublet lattice method.[5]

The experimental data used for the comparisons were obtained in a series of tests conducted by the National Aeronautics and Space Administation (NASA) in the Langley Transonic Dynamics Tunnel (TDT) using a rigid semispan model of a high-aspect-ratio supercritical wing equipped with oscillating control surfaces. The test results provide a comprehensive data base of measured subsonic and transonic, steady- and unsteady-pressure distributions for comparison and validation of applicable aerodynamic theories. The wind tunnel test conditions were varied in Mach and Reynolds numbers, and the semispan wing model was varied in angle of attack, control-surface deflection angle, and control-surface oscillation amplitude and frequency. The measured data presented herein are selected from tabular compilations published in two NASA technical memorandums.[6,7] The focus of the wind tunnel tests was to measure the unsteady pressures on the wing due to oscillating control surfaces at two trailing-edge semispan locations for both subsonic and transonic conditions. Two recent publications[8,9] present limited comparisons of these wind tunnel data with the linear lifting-surface aerodynamics of a kernel function method.[10]

The purpose of the present paper is to present comparative results of measured steady- and unsteady-pressure distributions with doublet lattice calculations at subsonic and transonic Mach numbers of 0.60 and 0.78, respectively. The doublet lattice method was chosen for the present study because of its extensive use within currently available com-

Presented as Paper 84-0301 at the AIAA 22nd Aerospace Science Meeting, Reno, Nev., Jan. 9-12, 1984; received May 21, 1984; revision received Nov. 15, 1984.

*Aerospace Engineer, Aeroservoelasticity Branch, Loads and Aeroelasticity Division. Member AIAA.

puter programs for active control synthesis and analysis. Detailed comparisons have been made at each of the two Mach number conditions and are published in two NASA technical memorandums.[11,12] Both differences and similarities between the measured and calculated data are presented herein for the two Mach number conditions, with emphasis on the comparisons of the pressure distributions produced by the two control surfaces. Some preliminary empirical corrections, based on steady-pressure measurements and applied to unsteady doublet lattice calculations at $M=0.78$, are also presented.

Models

Wind Tunnel Model

Details of the complete wind tunnel model configuration, which included a semispan wing and a half-body fuselage, are decribed in Refs. 6, 7, and 9. A sketch detailing the geometric properties of the wing planform is shown in Fig. 1. The wing has an aspect ratio of 10.76, a leading-edge sweepback angle of 28.8 deg, and a semispan of 2.286 m. The designated semispan stations for nine chordwise sets of static-pressure orifices are tabulated in Fig. 1. Static pressures were measured at 252 locations, and dynamic pressures at 164 locations. Both the static- and dynamic-pressure measurements were made at closely corresponding semispan locations on the wing. The static-pressure orifices and dynamic-pressure transducers were also installed at corresponding upper and lower surface locations to facilitate obtaining lifting-surface distributions directly.

Although a total of 10 independently oscillating control surfaces were available on the wing (five along the lead edge and five along the trailing edge), this study only considered the two trailing-edge control surfaces shown in Fig. 1: 1) the inboard control surface located between 10 and 24% semispan, and 2) the outboard control surface located between 59 and 79% semispan. Both control surfaces have hinge lines at 80% chord.

Doublet Lattice Model

An aerodynamic model was generated for use in the subsonic, unsteady, lifting-surface theory known as the doublet lattice method.[5] The arrangement of aerodynamic boxes representing the wind tunnel model is shown in Fig. 2. The aerodynamic boxes for the control surfaces and streamwise strips corresponding to the pressure measurement stations are identified in the figure. This doublet lattice model consists of 42 streamwise strips and a total of 325 aerodynamic boxes. In creating the aerodynamic box layout, an attempt was made to keep the aspect ratio of each box near unity, as recommended in Ref. 13. The doublet lattice model does not include an aerodynamic respresentation for the half-body fuselage of the wind tunnel model. Therefore, no wing-body effects are accounted for in the analysis. The relatively large number of aerodynamic boxes contained in this model, especially the high density of boxes both near and on the control surfaces, was chosen purposely to provide more detailed chordwise pressure points for comparative purposes.

Efficient use of computer resources is always important to reduce costs, especially in parametric and optimization studies using aerodynamic codes. Because this study required doublet lattice runs at only two Mach numbers and four reduced frequencies, the cost of the calculations was not prohibitive. A typical CPU time to execute the doublet lattice program with the box layout of Fig. 2 was approximately 600 s on a CDC® Cyber 175.† These runs required a maximum field length of about 130 K-octal. Numerous doublet lattice runs for

†The use of trade names in this publication does not constitute endorsement, either expressed or implied, by NASA.

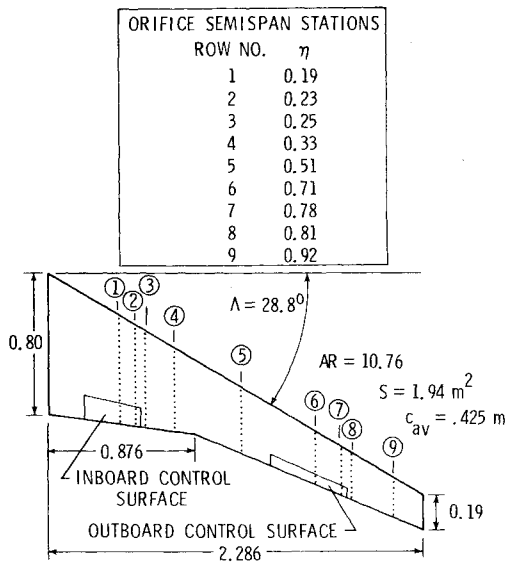

Fig. 1 Wing planform geometry and orifice semispan stations (linear dimensions in meters).

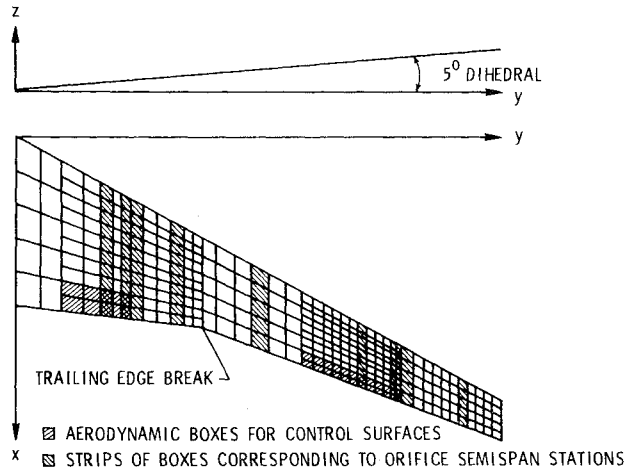

Fig. 2 Doublet lattice aerodynamic model.

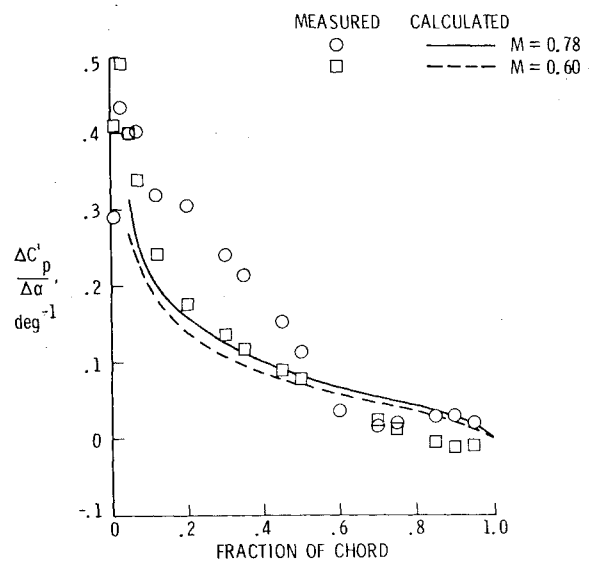

Fig. 3 Chordwise incremental steady-pressure distributions per incremental angle of attack ($\eta=0.51$).

parametric and optimization studies would require a model layout of fewer boxes to reduce computational time and costs.

Wind Tunnel Measurements

All of the wind tunnel measurements presented herein were obtained at freestream Mach numbers of 0.60 and 0.78, with respective freestream dynamic pressures of 3.0 and 3.9 kPa. The Reynolds number was 2.2 million based on the average wing chord.

Steady-Pressure Data

The steady-pressure measurements from Refs. 6 and 7 consist of tabulated steady-pressure coefficients, C_p, on both upper and lower surfaces of the wing with the corresponding lifting-surface steady-pressure coefficients, $C_p' = C_{p_{\text{l.s.}}} - C_{p_{\text{u.s.}}}$. The section lift coefficients, c_ℓ, at each of the nine semispan stations were obtained by numerically integrating Eq. (1).

$$c_\ell = \frac{1}{c}\int_0^1 C_p' dx \tag{1}$$

Calculations were also made for the incremental changes in those coefficients due to angle of attack or control-surface deflection changes, as follows:

$$\frac{\Delta c_\ell}{\Delta\alpha} = \frac{c_\ell - c_{\ell_{\text{ref}}}}{\alpha - \alpha_{\text{ref}}} \tag{2}$$

$$\frac{\Delta c_\ell}{\Delta\delta} = \frac{c_\ell - c_{\ell_{\text{ref}}}}{\delta - \delta_{\text{ref}}} \tag{3}$$

$$\frac{\Delta C_p'}{\Delta\alpha} = \frac{C_p' - C_{p_{\text{ref}}}'}{\alpha - \alpha_{\text{ref}}} \tag{4}$$

$$\frac{\Delta C_p'}{\Delta\delta} = \frac{C_p' - C_{p_{\text{ref}}}'}{\delta - \delta_{\text{ref}}} \tag{5}$$

The reference quantities correspond to the zero-valued test conditions ($\alpha_{\text{ref}} = 0$ deg and $\delta_{\text{ref}} = 0$ deg).

Unsteady-Pressure Data

The unsteady-pressure measurements from Refs. 6 and 7 consist of the magnitude of the lifting-surface unsteady-pressure coefficient $|C_p'|$ and phase angle ϕ. The magnitudes of the lifting-surface unsteady-pressure coefficients are presented in per-degree form (i.e., each was divided by the absolute value of the amplitude of control-surface deflection angle, $|C_p'|/|\delta|$). All phase angles are referenced to the control surface, with negative values for pressure changes lagging the control-surface motion. Each control surface was oscillated at a given amplitude about a mean deflection angle at three frequencies (5, 10, and 15 Hz). However, only 10 Hz data are presented herein. Depending on the exact tunnel speed for a given test point, the corresponding reduced frequencies varied slightly about average values of 0.14, 0.27, and 0.41 for the Mach 0.60 data, and 0.11, 0.21, and 0.32 for the Mach 0.78 data. The unsteady-pressure data used in this study were obtained for control-surface amplitudes of oscillation of ± 4 and ± 6 deg at Mach 0.60 and 0.78, respectively. Test conditions also included two angles of attack: 0 and 2.85 deg at Mach 0.60, and 0 and 2.05 deg at Mach 0.78. Although unsteady-pressure measurements were made at all nine semispan stations, only the chordwise distributions at two locations (near the center of each control surface) were considered in this study.

Doublet Lattice Calculations

The doublet lattice formulation solves the linearized acceleration or pressure potential-flow equation on zero-thickness, zero-cambered lifting surfaces at subsonic speeds with nonplanar boundary conditions. The present calculations were performed using the version of the doublet lattice program which resides in ISAC (Interaction of Structures, Aerodynamics, and Controls),[1] a system of several computer programs assembled together through a common data base.

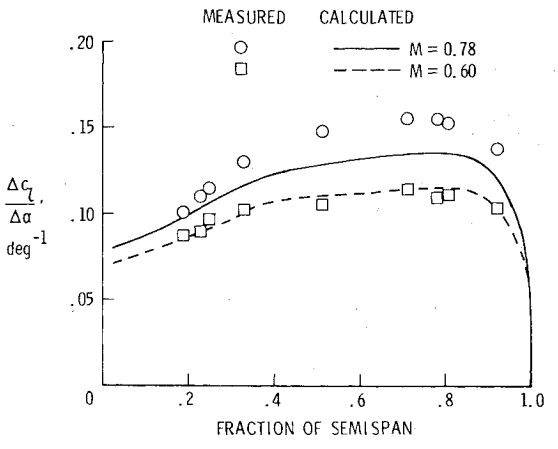

Fig. 4 Spanwise incremental steady lift distributions per incremental angle of attack.

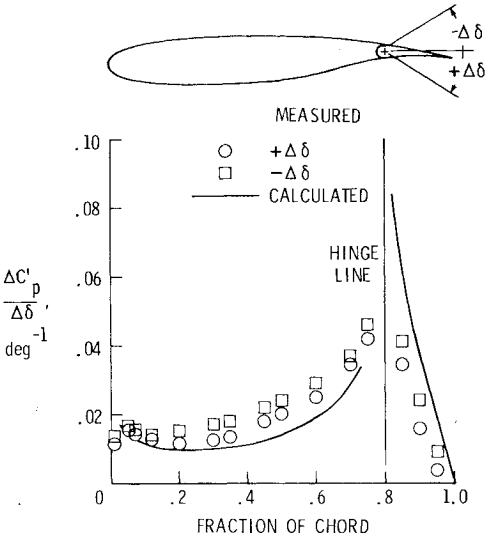

a) Subsonic comparison, $M = 0.60$, $\alpha = 2.85$ deg.

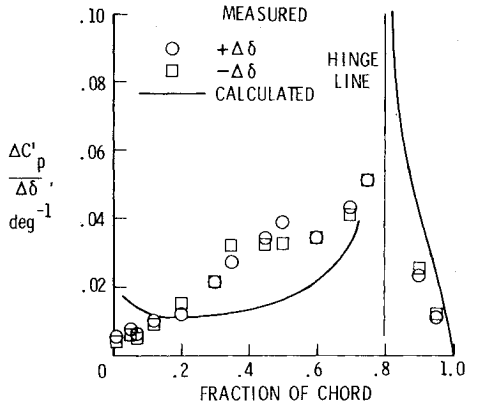

b) Transonic comparison, $M = 0.78$, $\alpha = 2.05$ deg.

Fig. 5 Chordwise incremental steady-pressure distributions due to inboard control-surface deflections ($\eta = 0.19$).

The wind tunnel model was essentially rigid and pressure-measurement results were not significantly influenced by model flexibility.[9] Therefore, pressure distributions due only to angle of attack and control-surface deflections were calculated. Reduced frequencies were chosen to correspond to those averages of the experimental data stated previously.

For each reduced frequency, the output from the doublet lattice program consists of complex lifting-surface pressure coefficients on each aerodynamic box. Since the program performs the necessary numerical integrations internally, the complex section lift coefficients are output directly. At zero reduced frequency (steady) the imaginary part of these complex quantities are zero. The real and imaginary parts of the unsteady quantities were converted to magnitudes (per degree) and phase angles for comparison to the measured values.

Comparison of Measured and Calculated Results

General

Steady-pressure comparisons of the measured data and the doublet lattice calculations include 1) chordwise incremental lifting-surface pressure distributions per incremental angle of attack and incremental control-surface deflection, and 2) spanwise incremental lift distributions per incremental angle of attack and incremental control-surface deflection. Unsteady-pressure results, due to the oscillating control surfaces, are shown in the form of lifting-surface unsteady-pressure coefficient magnitude and phase angle.

Steady-Pressure Results

The measured wind tunnel data presented herein are average values taken over representative sets of incremental test conditions. Incremental test conditions are model variations of angle of attack or control-surface deflection over a range of values with all other parameters held constant. Table 1 summarizes the test conditions over which the steady-pressure data were averaged. The measured steady pressures are reasonably linear over each set of incremental test conditions. The steady pressures due to control-surface deflections have been averaged separately over positive and negative deflection angles. This shows a particular difference in chordwise pressure distributions due to outboard control-surface deflections and will be discussed later. Detailed comparisons of chordwise pressure distributions were made in Refs. 11 and 12. The averaged data presented herein retain the same general trends and provide a more discernible comparison.

Figure 3 contains typical comparisons of chordwise incremental lifting-surface steady-pressure distributions per incremental angle of attack, for both subsonic and transonic speeds, at semispan station $\eta = 0.51$. The doublet lattice calculations underpredict the measured values forward of the midchord, and overpredict the measured values aft of the midchord. The differences between the measured and calculated data are typical of airfoil thickness effects.[14] The measured transonic data show a bulge in pressure between 0.20 and 0.50 fraction of chord due to the compression regions in the steady flow.

A comparison is shown in Fig. 4 of spanwise incremental steady lift distributions per incremental angle of attack. The subsonic comparison in very good. The measured transonic data are consistently underpredicted by the doublet lattice calculations, which is a direct result of the transonic pressure bulge shown previously in Fig. 3.

The chordwise incremental lifting-surface steady-pressure distributions per incremental control-surface deflections are shown in Figs. 5 and 6. The inboard control-surface data are presented in Fig. 5a and 5b for the subsonic and transonic comparisons, respectively. The outboard control-surface data are presented in Fig. 6. Each figure contains averages of the measured data for three positive and three negative incremental control-surface deflections ($\Delta\delta = \pm 2, \pm 4$ and ± 6 deg). The measured data were obtained at test conditions of about 2.85 and 2.05 deg angles of attack for the subsonic and transonic cases, respectively.

In the subsonic comparison of Fig. 5a both the measured and calculated data show similar trends. The measured

Table 1 Test conditions for average steady-pressure measurements

Constant test conditions		Incremental test conditions
		Angle of attack
M	δ, deg	$\Delta\alpha$, deg
0.60	0	2.85, 2.85
0.78	0	−3, −2, −1, 1, 2, 2.58, 3, 4,
		Inboard control surface
M	α, deg	$\Delta\delta$, deg
0.60	2.85	−6, −4, −2, 2, 4, 6
0.78	2.05	−6, −4, −2, 2, 4, 6
		Outboard control surface
M	α, deg	$\Delta\delta$, deg
0.60	2.85	−6, −4, −2, 2, 4, 6
0.78	2.05	−6, −4, −2, 2, 4, 6

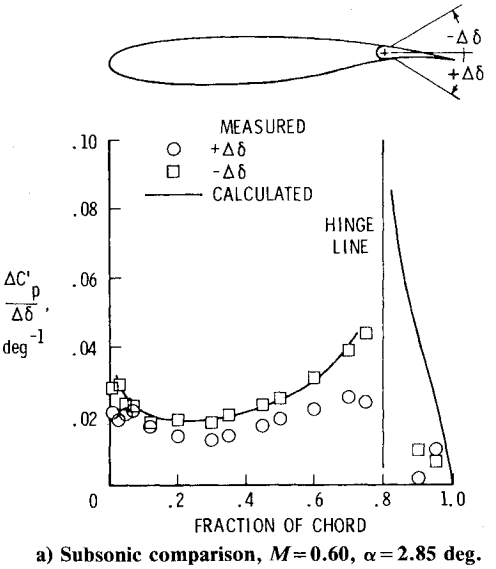

a) Subsonic comparison, $M = 0.60$, $\alpha = 2.85$ deg.

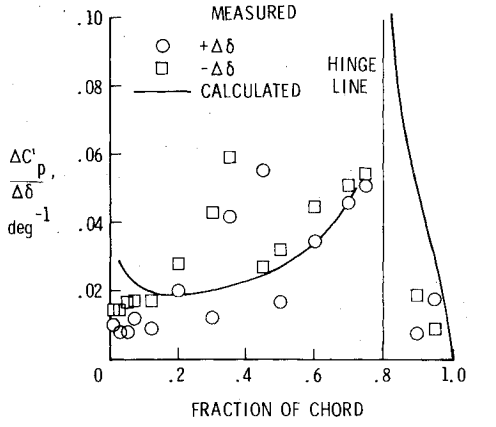

b) Transonic comparison, $M = 0.78$, $\alpha = 2.05$ deg.

Fig. 6 Chordwise incremental steady-pressure distributions due to outboard control surface deflections ($\eta = 0.71$).

magnitudes due to positive control-surface deflections are slightly less than those due to negative deflections. The transonic comparisons in Fig. 5b display two features indicative of transonic effects in the measured data: 1) a reduction in magnitude of the measured pressures near the leading edge as compared to the predicted rise in the doublet lattice calculations, and 2) the bulge in the measured pressures near the midchord as compared to the doublet lattice calculations. For both the subsonic and transonic comparisons of the inboard control-surface data, the doublet lattice calculations overpredict the measured chordwise pressure distributions aft of the control-surface hinge line. However, the measured and calculated data do show similar trends.

The measured outboard control-surface data, at both the subsonic and transonic conditions, exhibited possible separated flow toward the trailing edge due to positive deflections. There was a rise in the steady-pressure distribution at the 95% chord location after a drop in pressure at the 90% chord location, as shown in Fig. 6. In comparing the measured data in Fig. 6b with the measured data of Fig. 5b, there are large excursions outboard (for both positive and negative deflections) which do not occur inboard. This suggests the greater sensitivity in the outboard regions of flow is due to the stronger shocks there, as opposed to the weaker shocks found inboard. In general, the inboard control-surface comparisons illustrate some expected discrepancies between linear theory and experiment with well-behaved or smooth changes in the measured chordwise pressure distributions. In contrast, the outboard control-surface comparisons show discrepancies between the measured and calculated pressure distributions that are not as well behaved, especially at the transonic condition.

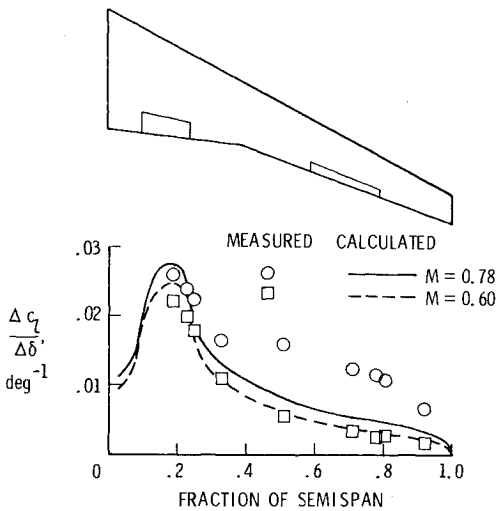

a) Inboard control surface.

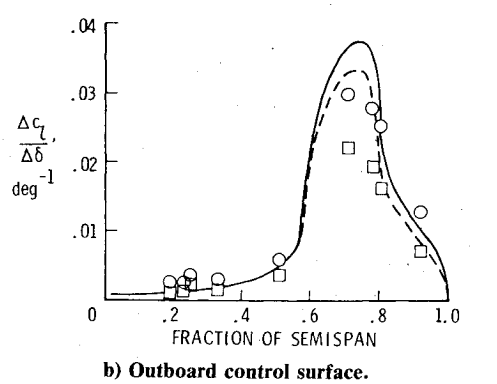

b) Outboard control surface.

Fig. 7 Spanwise incremental lift distributions per incremental control-surface deflections.

The spanwise distributions of section lift coefficients for both inboard and outboard incremental control-surface deflections are shown in Figs. 7a and 7b, respectively. The average values of the measured data were taken over six incremental control-surface deflections. In Fig. 7a, for $m = 0.60$, the doublet lattice program predicted the steady lift distributions over the entire semispan very well. For $m = 0.78$, there is good agreement to about 0.25 semispan, outboard of which the doublet lattice calculations underpredict the measured data consistently. The exact cause of this anomaly is not understood at the present time, but is likely a result of three-dimensional transonic effects. The measured subsonic and transonic data for the outboard control-surface deflections, shown in Fig. 7b, are significantly overpredicted by the doublet lattice calculations near the midspan of the outboard control surface, $\eta = 0.71$. Elsewhere over the semispan, the doublet lattice calculations agree quite well with the measured data.

Unsteady-Pressure Results

The measured unsteady-pressure data presented herein are values averaged over two angles of attack at each Mach number (0 and 2.85 deg at $M = 0.60$, 0 and 2.05 deg at $M = 0.78$). As shown in Refs. 11 and 12, there were only minor

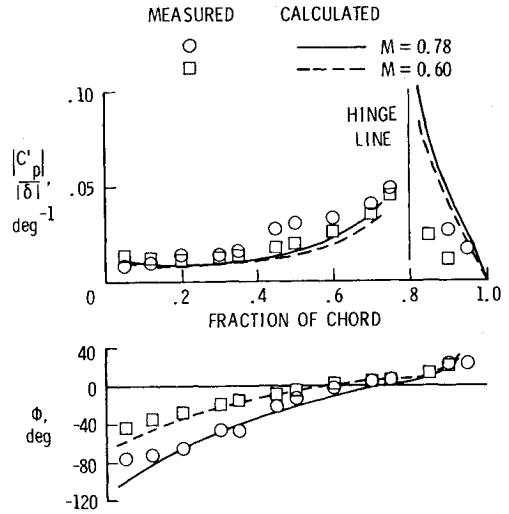

Fig. 8 Chordwise unsteady-pressure distributions due to oscillating inboard control surface ($\eta = 0.19$, $f = 10$ Hz).

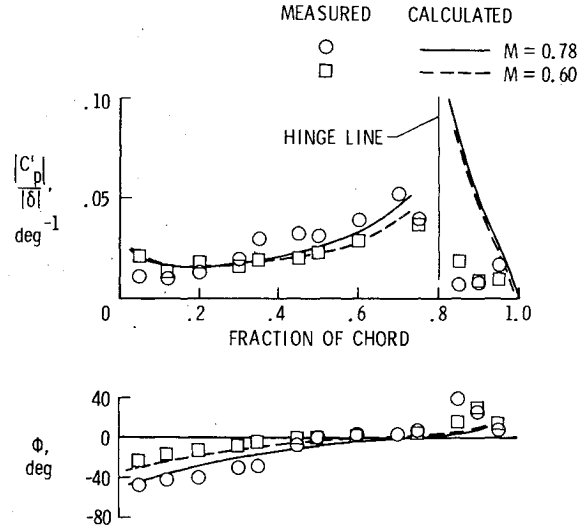

Fig. 9 Chordwise unsteady-pressure distributions due to oscillating outboard control surface ($\eta = 0.71$, $f = 10$ Hz).

differences in the chordwise lifting-surface unsteady-pressure measurements at these two angles of attack.

Comparisons of the chordwise lifting-surface unsteady-pressure distributions in the form of magnitude and phase angle are presented in Figs. 8 and 9 for the inboard and outboard oscillating control surfaces, respectively. Similar to the steady-pressure magnitudes is the doublet lattice overprediction aft of each control surface hinge line. The bulge in measured pressures near the midchord at the transonic condition is again apparent. Although overpredicted aft of the hinge line, the measured unsteady-pressure magnitudes in Fig. 8 follow the same trend as the doublet lattice calculations. The measured and calculated phase angles in Fig. 8 compare very well along the chordwise distributions, except near the leading edge. The measured magnitudes near the trailing edge ($x/c=0.90$ and 0.95) of the outboard control surface, as shown in Fig. 9, exhibit the same separated flow effect as previously shown in the steady-pressure data. At these same trailing-edge locations of the outboard control surface, there are noticeable deviations between the measured and calculated phase angles. In general, the phase angle calculations shown in Figs. 8 and 9 are considered good, even at the transonic condition, $M=0.78$.

Corrections to Calculated Results

One of the objectives of this comparative study was to help develop and verify empirical corrections to the doublet lattice calculations. The limitations of the doublet lattice method, as well as other linear lifting-surface theories at transonic conditions, are well known and illustrated by the results presented so far. Consequently, corrections are routinely employed to make improvements to the calculated aerodynamics based on experimental measurements. Such adjustments to linear aerodynamic analysis cannot be regarded as addressing any of the fundamental causes of the discrepancies. The following preliminary corrections are presented only for the inboard and outboard control-surface data at $M=0.78$, since the differences between measured and calculated data are more pronounced at the transonic condition.

The doublet lattice formulation is a finite element or discretized lifting-surface method, such that the resultant matrix of aerodynamic influence coefficients (AIC) can be modified easily with premultiplier and/or postmultiplier matrices. Premultiplier correction factors can be considered as adjustments to the pressure distribution, and postmultiplier correction factors can be considered as adjustments to the downwash. The discrepancies between experiment and theory in predicting trailing-edge control-surface loads are usually considered to be due to boundary-layer displacement effects on the effective downwash. Therefore, postmultiplier correction factors commonly are used to correct doublet lattice calculations for trailing-edge control-surface loads.[15] However, postmultiplier correction factors usually affect both the real and imaginary parts of the downwash, thus changing the phase angles of the pressures. Premultiplier correction factors affect the pressure magnitudes, and not the phase angles.

As shown in the preceding comparisons of the chordwise steady-pressure data, a change in the theoretical pressure distributions could simultaneously address the transonic bulge in the measured pressures near the midchord, and the drop in measured pressures near the leading edge and aft of the control-surface hinge lines. Although results are not presented, several postmultiplier correction factors were applied to the doublet lattice calculations and none proved to be satisfactory. The magnitudes of the unsteady-pressure distributions were not changed substantially from their original values, and their chordwise trend remained unchanged. However, of more significance, the postmultiplier correction factors usually worsened the phase angle calculations as compared to the measured values. However, a set of premultiplier correction factors was selected which improved

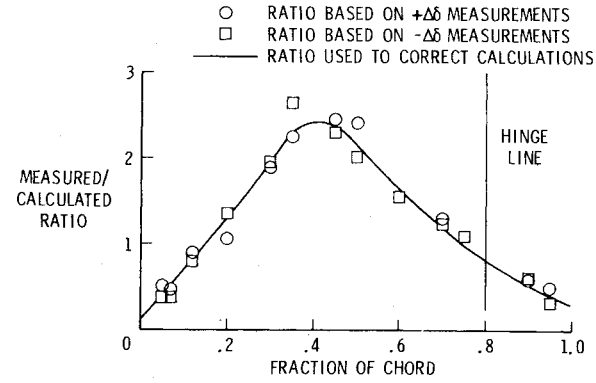

a) Inboard control surface, $\eta=0.19$.

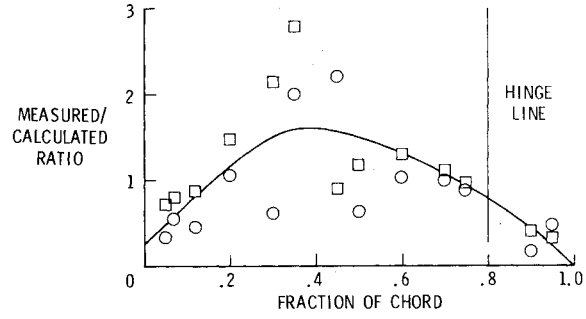

b) Outboard control surface, $\eta=0.71$.

Fig. 10 Ratios of measured to calculated chordwise steady-pressure distributions due to control-surface deflections ($M=0.78$).

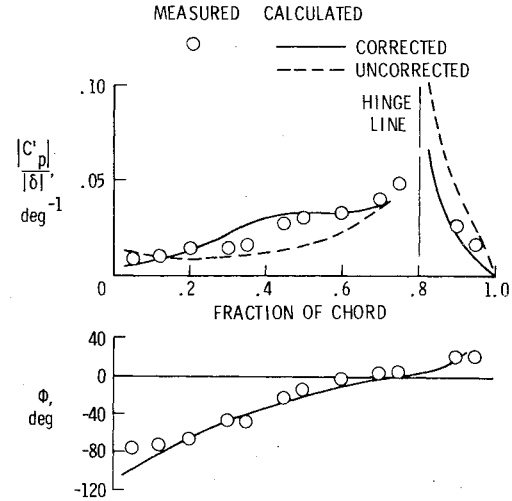

Fig. 11 Corrected and uncorrected calculations with measured chordwise unsteady-pressure distributions due to oscillating inboard control surface ($M=0.78$, $\eta=0.19$, $f=10$ Hz).

the calculations. The following discussion addresses these results.

The ratios of measured chordwise steady-pressure distributions to the doublet lattice calculations for the inboard and outboard control-surface data are shown in Figs. 10a and 10b, respectively. Note the well-behaved trend of the ratios to the more erratic behavior for the outboard data. This again highlights the sensitivity of the measured outboard control surface pressures to positive or negative deflections. Correction factors were obtained by fitting a smooth curve through the chordwise distribution of ratios and choosing values at locations corresponding to the midchords of aerodynamic

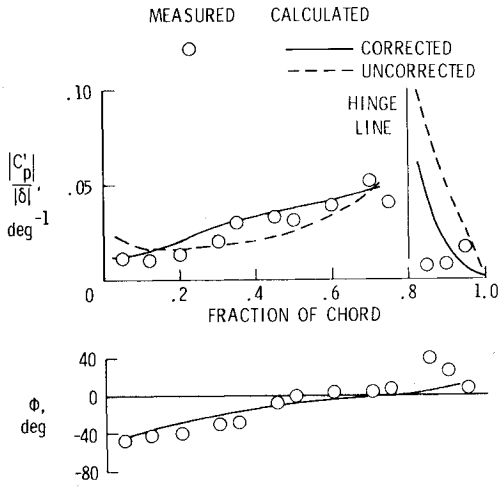

Fig. 12 Corrected and uncorrected calculations with measured chordwise unsteady-pressure distributions due to oscillating outboard control surface ($M=0.78$, $\eta=0.71$, $f=10$ Hz).

boxes in a steamwise strip. For this study, the correction factors were applied only to aerodynamic boxes in streamwise strips with control surfaces. Figures 11 and 12 show the calculated chordwise unsteady-pressure distributions which result from applying the respective correction factors for each control surface. As stated previously, the calculated phase angles are not changed by the premultiplier correction factors. The comparison of corrected doublet lattice calculations with measured chordwise unsteady-pressure distributions is better than that of uncorrected calculations. Although the empirical corrections to the unsteady aerodynamics are applicable only to the configuration herein at $M=0.78$, the basis of their derivation from steady-pressure measurements provides a useful method for similar applications.

Concluding Remarks

A comparative study of measured and calculated airloads has been made for a high-aspect-ratio supercritical wing model representative of an energy-efficient transport wing. The calculated airloads were obtained using the unsteady aerodynamic lifting-surface theory known as the doublet lattice method. Steady-pressure comparisons were made for incremental changes in angle of attack and control-surface deflections. The measured steady and unsteady aerodynamics show some expected deviations from the calculated values, especially at the transonic condition, since viscous and transonic effects are not accounted for in the doublet lattice analysis.

The measured chordwise steady-pressure distributions due to incremental angles of attack are underpredicted forward of the midchord by the doublet lattice calculations and overpredicted aft of the midchord (typical of thickness effects). Transonic effects in the measured Mach 0.78 data are evident by the bulge in chordwise steady-pressure distributions. The transonic effects result in the doublet lattice program underpredicting the spanwise lift distribution due to the incremental angles of attack. The measured chordwise steady-pressure distributions due to control-surface deflections are overpredicted by the doublet lattice calculations aft of both control-surface hinge lines. This discrepancy is worse for the outboard control-surface data due to possible separated flow conditions at the trailing edge. There is also a signficant underprediction of the transonic spanwise incremental lift distribution per incremental inboard control-surface deflection, over the semispan stations outboard of the inboard control surface.

The chordwise unsteady-pressure comparisons show particularly good agreement between the measured and calculated phase angles. The measured unsteady-pressure magnitudes, however, are noticeably overpredicted aft of each control-surface hinge line. In general, the unsteady-pressure magnitude comparisons are very similar to the steady-pressure comparisons. The differences shown between measured data and doublet lattice predictions can be adjusted empirically. Empirical correction factors based on the measured steady-pressure distributions are applied to the unsteady aerodynamic calculations. Results of the empirically corrected unsteady pressures at $M=0.78$ show a considerable improvement to the doublet lattice predictions. This empirical method has the advantage of improving unsteady calculations without the time and expense of performing wind tunnel tests for unsteady-pressure measurements. Empirical corrections to linear unsteady aerodynamic calculations are only near term and necessary, until nonlinear unsteady transonic aerodynamic calculations are readily available.

References

[1]Peele, E.L. and Adams, W.M. Jr., "A Digital Program for Calculating the Interaction Between Flexible Structures, Unsteady Aerodynamics and Active Controls," NASA TM 80040, 1979.

[2]Adams, W.M. Jr. and Tiffany, S.H., "Control Law Design to Meet Constraints Using SYNPAC—Synthesis Package for Active Controls," NASA TM 83264, 1982.

[3]Perry, B. III, Kroll, R.I., Miller, R.D., and Goetz, R.C., "DYLOFLEX—A Computer Program for Flexible Aircraft Flight Dynamic Loads Analyses with Active Controls," *Journal of Aircraft,* Vol. 17, April 1980, pp. 275-282.

[4]Nissim, E. and Abel, I., "Development and Application of an Optimization Procedure for Flutter Suppression Using the Aerodynamic Energy Concept," NASA TP 1137, 1978.

[5]Giesing, J.P., Kalman, T.P., and Rodden, W.P., "Subsonic Unsteady Aerodynamics for General Configurations, Part I, Vol. I—Direct Application of the Nonplanar Doublet Lattice Method," AFDDL-TR-71-5, Nov. 1971.

[6]Sandford, M.C., Ricketts, R.H., and Cazier, F.W. Jr., "Transonic Steady- and Unsteady-Pressure Measurements on a High-Aspect-Ratio Supercritical-Wing Model with Oscillating Control Surfaces," NASA TM 81888, 1980.

[7]Sandford, M.C., Ricketts, R.H., and Watson, J.J., "Subsonic and Transonic Pressure Measurements on a High-Aspect-Ratio Supercritical-Wing Model with Oscillating Control Surfaces," NASA TM 83201, 1981.

[8]Sandford, M.C., Ricketts, R.H., Cazier, F.W. Jr., and Cunningham, H.J., "Transonic Unsteady Airloads on an Energy Efficient Transport Wing with Oscillating Control Surfaces," *Journal of Aircraft,* Vol. 18, July 1981, pp. 557-561.

[9]Watson, J.J., "Elastic Deformation Effects on Aerodynamic Characteristics for a High-Aspect-Ratio Supercritical-Wing Model," NASA TM 83286, 1982.

[10]Rowe, W.S., Sebastian, J.D., and Petrarca, J.R., "Reduction of Computer Usage Costs in Predicting Unsteady Aerodynamic Loadings Caused by Control Surface Motions—Analysis and Results," NASA CR-3009, 1979.

[11]McCain, W.E., "Comparison of Analytical and Experimental Subsonic Steady- and Unsteady-Pressure Distributions for a High-Aspect-Ratio Supercritical Wing Model with Oscillating Control Surfaces," NASA TM 84490, 1982.

[12]McCain, W.E., "Comparison of Analytical and Experimental Steady- and Unsteady-Pressure Distributions at Mach Number 0.78 for a High-Aspect-Ratio Supercritical Wing Model with Oscillating Control Surfaces," NASA TM 84589, 1983.

[13]Giesing, J.P., Klaman, T.P., and Rodden, W.P., "Subsonic Unsteady Aerodynamics for General Configurations, Part I, Vol. II—Computer Program H7WC," AFFDL-TR-71-5, Nov. 1971.

[14]Rowe, W.S., Redman, M.C., Ehlers, F.E., and Sebastion, J.D., "Prediction of Unsteady Aerodynamic Loadings Caused by Leading Edge and Tailing Edge Control Surface Motions in Subsonic Compressible Flow—Analysis and Results," NASA CR-2543, 1975.

[15]Giesing, J.P., Kalman, T.P., and Rodden, W.P., "Correction Factor Techniques for Improving Aerodynamic Prediction Methods," NASA CR-144967, 1976.